Air separation by silver titanosilicate with enhanced density

M. Shi, A.M. Avila, L. Wu, J.A. Sawada, T.M. Kuznicki, S.M. Kuznicki *

Department of Chemical and Materials Engineering, University of Alberta, Edmonton, Alberta T6G 2V4, Canada

ARTICLE INFO

ABSTRACT

Previously, we reported that Ag-ETS-10 can be used to separate air, and produce argon free oxygen. It was reported that high purity oxygen (99+%) was generated using a bed of Ag-ETS-10 granules to separate air (78.0% N_2, 21.0% O_2, 1.0% Ar) at 25 °C and 100 kPa, with an O_2 recovery larger than 30%. In this study, a higher oxygen recovery was achieved by enhancing the capacity of the adsorbent material and by improving the packing efficiency of the adsorbent within the granules. The packing efficiency of the bed was increased through the combination of two different granule sizes. Here we report a lab scale demonstration of high purity oxygen (99+%) production by adsorptive air separation (78.0% N_2, 21.0% O_2, 1.0% Ar) with an O_2 recovery approaching 40%. Further improvements in oxygen recovery are possible due to the exceptional crystalline density of Ag-ETS-10 ($\sim$3.84 g/cm^3).

© 2013 Elsevier B.V. All rights reserved.

1. Introduction

Oxygen is one of the best-known and most widely used chemicals [1], with diverse applications in almost every branch of industry. Nearly 100 million tons of oxygen are consumed every year making the separation of oxygen from air an extremely large and important business [2]. The oxygen market is expected to grow significantly as all large-scale clean energy technologies of the future will require oxygen as a feed [3–5].

High purity oxygen (99+%) is required in many applications such as welding and cutting processes [6], plasma chemistry [7,8], rocket propulsion systems [9] and semiconductor manufacturing [10]. In order to meet the demand for high purity oxygen in a cost-effective manner the oxygen recovery from air needs to be optimized.

Currently, two fundamentally different approaches are used for air separation: cryogenic and non-cryogenic processes. Typically, cryogenic distillation is used in applications that require large (tons) quantities of oxygen at ultra-low temperatures. Non-cryogenic air separation processes include pressure swing adsorption (PSA) and membrane processes [11]. PSA utilizes molecular sieve adsorbents to fraction the components in air. Polymeric membranes are used for ambient temperature separations [12,13] while specialized ceramic membranes (oxygen ion transport membranes) require elevated temperatures to selectively separate O_2 from air [14,15].

High-purity oxygen can be obtained by PSA using air as a feed (78.0% N_2, 21.0% O_2, 1.0% Ar) at 25 °C and 100 kPa on a bed of Ag-ETS-10 granules [16,17]. The principal operating cost for a PSA air separation unit is the electricity used to run the compressor. A PSA process operating at a low O_2 recovery will require a larger volume of feed air to achieve a fixed product flow rate. Larger feed volumes of air, in turn, require an increase in the size and cost of the feed compressor and use more energy per mass of O_2. From a materials perspective, high purity oxygen recovery can be enhanced by increasing the Ar/O_2 adsorption selectivity of the molecular sieve. The recovery of oxygen could also be enhanced by increasing the density of the adsorbent granules. The density of Na/K-ETS-10 crystals [18] is equal to 2.5 g/cm^3 but the as-synthesized ETS-10 powder [19] has a measured bulk density of only 0.78 g/cm^3. Through optimization of the synthesis conditions ETS-10 crystal morphology can be altered in such a way that increases the bulk density of the resulting granules. In addition, mixed packing of particles of two different sizes can further enhance the density of the adsorbent bed. Smaller particles fill the interspaces created by larger particles and the bed porosity is reduced.

This study focuses on increasing the recovery of high purity O_2 using Ag-ETS-10 obtained through density improvements to both the adsorbent powder and adsorbent bed. The production and recovery yield of oxygen due to these changes was evaluated experimentally and compared with the results obtained for the regular density adsorbent. Integral mass balances in the adsorbent column for oxygen were used to analyze the dependency of the single-step pure oxygen recovery on the process variables.

* Corresponding author. Tel.: +1 780 492 8819; fax: +1 780 492 8958.
E-mail address: steve.kuznicki@ualberta.ca (S.M. Kuznicki).

2. Experimental

2.1. Sample preparation

Both regular ETS-10 (ETS-10-R) and high density ETS-10 (ETS-10-HD) samples were synthesized using conventional hydrothermal synthesis. The regular ETS-10 with low density was synthesized as reported by Kuznicki [19]. The synthesis of ETS-10-HD was performed hydrothermally in 125 mL Teflon-lined autoclaves (Parr instruments) with composition molar ratio of 5.5 SiO_2:3.0 Na_2O:1.5 K_2O:TiO_2:(300–800) H_2O at 200 °C (crystallization conditions) for 10 days.

The modified procedure for synthesis of ETS-10-HD followed these steps:

(1) 0.9 g of sodium hydroxide (97% + NaOH, Fisher) and 1.4 g of potassium hydroxide (85% + KOH, Fisher) were mixed in 64 g of de-ionized water (resistivity > 18 MΩ cm).
(2) Obtained mixture was then added to 9.5 g of sodium silicate (28.8% SiO_2, 9.14% Na_2O, Fisher), followed by the addition of 6.4 g of titanium trichloride (20% w/w solution in 2 N hydrochloric acid, Fisher).
(3) 0.1 g of ETS-10-R was seeded into the mixture. The pH of the mixture was adjusted to 10.1–10.3 by using HCl [1 M].
(4) Finally, the reaction mixture was sealed into an autoclave and reacted at 200 °C for 10 days. The autoclave was quenched to ambient temperature. The precipitate was washed and filtered by de-ionized water, and then dried in a forced-air oven at 80 °C for 24 h to produce ETS-10-HD.

On the basis of these materials (ETS-10-R and ETS-10-HD) two more adsorbents were prepared. Both as-synthesized ETS-10 samples were further Ag^+ exchanged by adding 5 g of ETS-10-HD (ETS-10-R) to 10 g of silver nitrate (Fisher, USP) in the presence of 50 g of deionized water. The mixtures were then heated to 80 °C for 1 h. The silver exchanged materials were filtered, washed with deionized water and the exchanged procedure was repeated two more times (for a total of three exchanges). The obtained Ag-ETS-10-R and Ag-ETS-10-HD were air dried for 24 h at 80 °C.

2.2. Characterization

Phase identification of ETS-10-R and ETS-10-HD was conducted by X-ray powder diffraction analysis (XRD) using a Rigaku Geigerflex 2173 with a vertical goniometer equipped with a graphite monochromator for filtration of $K–\beta$ wavelengths. Scanning electron microscopy (SEM) was performed on a Hitachi S2700 equipped with an X-ray EDS detector.

2.3. Density evaluation

Powder samples of ETS-10-R, ETS-10-HD, Ag-ETS-10-R and Ag-ETS-10-HD were pelletized by compressing quantities of powder in a 1″ diameter die pellet press to 69,000 kPa for 3 min. The resulting disks were crushed and sieved to obtain 20–50 and 10–16 mesh cuts. Mixed granule beds were prepared by thoroughly blending 50 wt% of 20–50 mesh size granules and 50 wt% of 10–16 mesh size granules. The measurements of the bulk density for the ETS-10 powders and granules were done according to the tap density procedure based on ISO standards [20].

2.4. Adsorption isotherms

The N_2, O_2 and Ar single adsorption isotherms on Ag-ETS-10-R and Ag-ETS-10-HD were measured at 25 °C using a volumetric adsorption analyzer (Micromeritics). Prior to adsorption tests adsorbent materials in crystalline powder form (with no added binders or diluents) were degassed at 250 °C for 2 h under vacuum.

2.5. Laboratory-scale demonstration

The schematics of the laboratory-scale setup for air separation on a molecular sieve are discussed in an earlier paper [21]. The breakthrough experiments were performed identically for both high density Ag-ETS-10-HD and low density (Ag-ETS-10-R) adsorbent beds. The adsorbent was packed into a 150 mL cylindrical stainless steel chamber with an inner diameter of 20 mm and a length of 450 mm. The columns packed with adsorbent pellets were activated at 200 °C for 10 h under 100 cm^3/min of helium flow.

The breakthrough experiments were run by conditioning the bed at 100 kPa with helium to purge any adsorbed gas from the system. The column temperature was maintained at 25 °C using a water cooling coil around the bed coupled to a circulating water bath. Dry air was fed into the fixed-bed column at a flow rate of 120 cm^3/min (P = 101.3 kPa, T = 25 °C) and the outlet gas composition was analyzed every 1 min using the adapted Varian 3800 gas chromatograph (GC). Outlet gas flow rate was monitored using flow meter Agilent ADM 1000. The Agilent flow meter was calibrated using a Bronkhorst mini CORI-FLOW™. Oxygen, argon and nitrogen composition analysis was performed on a modified Varian 3800 GC equipped with a thermal conductivity detector (TCD) as reported by Shi et al. [21].

2.6. Theoretical analysis of breakthrough times and high purity O_2 recovery

An integral molar balance for each species in the adsorption column can be expressed as

$$\int_0^\infty (F_{in,j} - F_{out,j})dt = q_j^* \rho_b V_b + C_j V_b \epsilon_b \tag{1}$$

where $F_{in,j}$ and $F_{out,j}$ are the molar flow rates in the column inlet and outlet respectively; q_j^* is the adsorbate concentration in equilibrium with the gas phase molar concentration in the feed, C_j; V_b, ρ_b and ϵ_b are the volume, density and porosity of the bed, respectively.

From Eq. (1) the mean residence time or mean breakthrough time $t_{bk,j}$ can be calculated [22] as

$$t_{bk,j} = \int_0^\infty \left(1 - \frac{F_{out,j}}{F_{in,j}}\right)dt = \frac{L}{v}\left(\frac{q_j^* \rho_b}{C_j} + \epsilon_b\right) \tag{2}$$

where L is the bed length and v represents the superficial velocity.

Considering that the mass transfer zones in the ternary mixture breakthroughs travel as shock waves (shock wave approximation [22,23]), the mass balance for O_2 can be expressed as:

$$\int_0^{t_{bk,N_2}} F_{in,O_2}dt - \int_{t_{bk,O_2}}^{t_{bk,Ar}} F_{out,O_2}dt - \int_{t_{bk,Ar}}^{t_{bk,N_2}} F_{out,O_2}dt$$
$$= q_{O_2}^* \rho_b V_b + C_{O_2} V_b \epsilon_b = F_{in,O_2} t_{bk,O_2} \tag{3}$$

from where t_{bk,O_2} is equal to:

$$t_{bk,O_2} = \int_0^{t_{bk,N_2}} \left(1 - \frac{F_{out,O_2}}{F_{in,O_2}}\right)dt \tag{4}$$

The argon-free O_2 recovery is expressed as

$$O_2 \text{ recovery} = \frac{\int_{t_{bk,O_2}}^{t_{bk,Ar}} F_{out,O_2}dt}{F_{in,O_2} \times t_{bk,Ar}} \tag{5}$$

By using the O_2 molar balance Eq. (3) along with the mean breakthrough time definition, the pure O_2 recovery can be expressed as
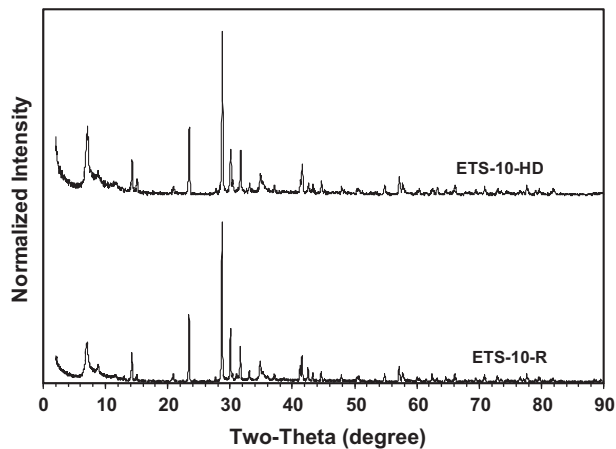
Fig. 1. XRD patterns of the regular ETS-10-R and high density ETS-10-HD adsorbents.

$$O_2 \ recovery = \frac{t_{bk,Ar} - t_{bk,O_2}}{t_{bk,Ar}} + \left(\frac{F_{out,O_2} - F_{in,O_2}}{F_{in,O_2}} \right) \left(\frac{t_{bk,Ar} - t_{bk,O_2}}{t_{bk,Ar}} \right) \quad (6)$$

Thus, pure O_2 recovery depends on the ratio between t_{bk,O_2} and $t_{bk,Ar}$. Using Eq. (2), Eq. (6) can be expressed as

$$O_2 \ recovery = \frac{F_{out,O_2}}{F_{in,O_2}} \left(1 - \frac{\frac{q_{O_2}^* \rho_b}{C_{O_2}} + \epsilon_b}{\frac{q_{Ar}^* \rho_b}{C_{Ar}} + \epsilon_b} \right) \quad (7)$$

By expressing it in terms of ρ_b

$$O_2 \ recovery = \frac{F_{out,O_2}}{F_{in,O_2}} \left(\frac{\rho_b (K_{Ar}^* - K_{O_2}^*)}{\rho_b K_{Ar}^* + \epsilon_b} \right)$$
$$= \frac{F_{out,O_2}}{F_{in,O_2}} \left(\frac{\rho_b (K_{Ar}^* - K_{O_2}^*)}{1 + \rho_b (K_{Ar}^* - \frac{1}{\rho_c})} \right) \quad (8)$$

where $K_{Ar}^* = \frac{q_{Ar}^*}{C_{Ar}}$ and $K_{O_2}^* = \frac{q_{O_2}^*}{C_{O_2}}$ are the corresponding equilibrium adsorption affinities of Ar and O_2 in the ternary mixture (N_2, O_2, Ar).

Considering ρ_b and K_{Ar}^* are moderate values (i.e., $\rho_b K_{Ar}^* + \epsilon_b > \rho_b K_{Ar}^*$), the recovery could be further enhanced by improving the packing efficiency inside the bed, i.e., increasing the bed density of the adsorbent material (ρ_b in Eq. (8)).

3. Results and discussion

3.1. Density enhancement

Fig. 1 shows that the XRD patterns of ETS-10-R and ETS-10-HD are equivalent and they both conform to the pattern reported by Kuznicki [19] for ETS-10. Fig. 2 shows SEM images of different magnifications of the crystallite morphology for both ETS-10-R and ETS-10-HD adsorbents. Typically, the observed ETS-10 crystals resembled truncated bi-pyramids with square basal planes shared by the two pyramids [18,24]. Surfaces of both ETS-10-R and ETS-10-HD samples possess the same characteristics. The as-synthesized low density ETS-10-R, however, has a more cubic shape and shows signs of some defects on the surface. The crystals of high density ETS-10-HD are anisotropic compared to ETS-10 and have no visible defects on their surfaces. This new morphology of ETS-10-HD crystals resulted in a higher bulk density and allowed more efficient packing within the adsorption column. Both XRD and SEM
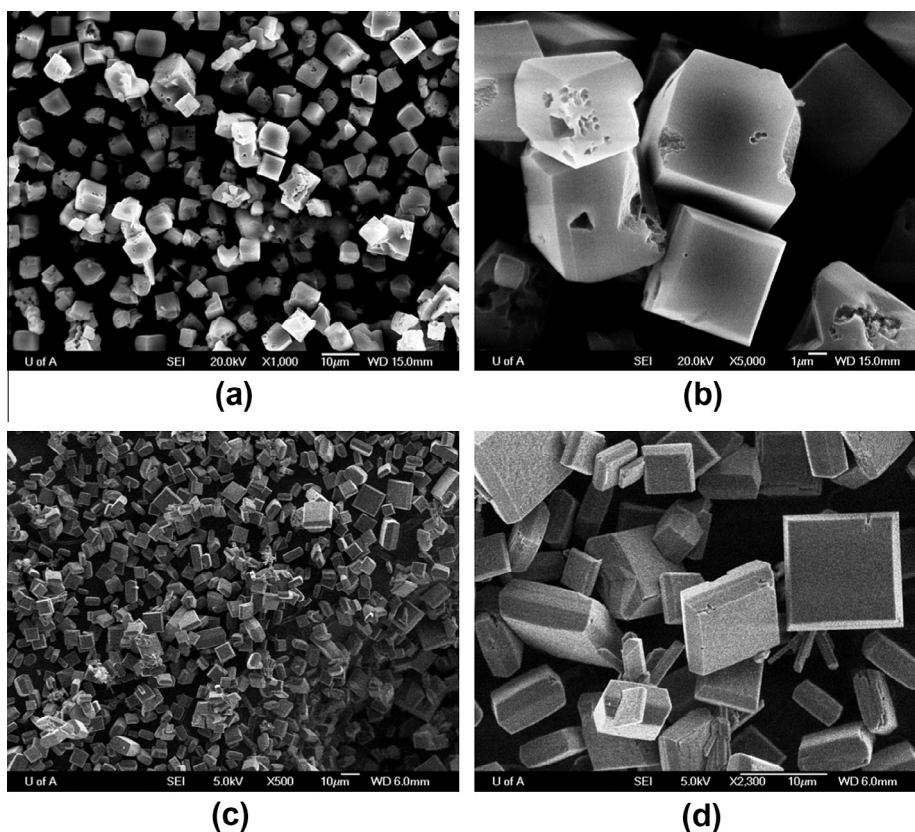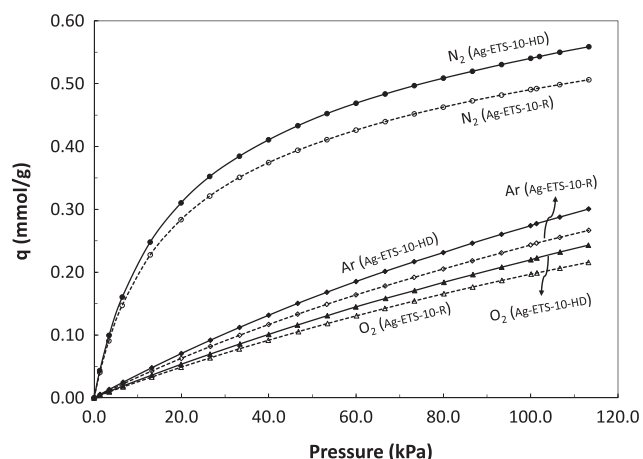

Fig. 2. SEM images of (a) ETS-10-R under 1000 magnification, (b) ETS-10-R under 5000 magnification, (c) ETS-10-HD with 500 magnification and (d) ETS-10-HD with 2300 magnification.

Fig. 3. Single adsorption isotherms of N_2, O_2 and Ar on Ag-ETS-10-R and Ag-ETS-10-HD at 25 °C.

Table 1
Bulk densities (g/cm^3) of ETS-10-based and Ag-ETS-10-based adsorbent materials.

	Powder (<0.044 mm)	Particles (1.19–2.00 mm)	Particles (0.297–0.841 mm)	50/50 Mixed particle
ETS-10-R	0.78	0.71	0.74	0.85
ETS-10-HD	0.95	0.87	0.88	1.01
Ag-ETS-10-R	1.00	0.93	0.95	1.12
Ag-ETS-10-HD	1.23	1.18	1.20	1.45

results confirm that the newly synthesized ETS-10-HD adsorbent possess the same ETS-10 structure as reported in the literature.

Fig. 3 shows the single component adsorption isotherms for the individual components of air on Ag-ETS-10-R and Ag-ETS-10-HD respectively. The enhancement of the synthesized material increased the adsorption capacity of the individual components. This might be attributed to the formation of less defective crystals in Ag-ETS-10-HD in comparison to Ag-ETS-10-R adsorbent (Fig. 2).

Table 1 shows the bulk densities for ETS-10-R, ETS-10-HD, Ag-ETS-10-R and Ag-ETS-10-HD samples in different forms: powder, 10–16 mesh size particles, 20–50 mesh size particles, and mixed size granules. The data indicates that a significant increase in density can be achieved by changing the synthesis conditions and tailoring the column packing using a wider cut of granules. The 150 mL adsorbent bed can contain either 130 g of low density Ag-ETS-10-R with 10–16 mesh size or 175 g of high density Ag-ETS-10-HD with mixed size granules (50% of 10–16 mesh and 50% of 20–50 mesh). The two approaches mentioned above resulted in 34.6 wt% increase of Ag-ETS-10-HD packing in a fixed volume.

3.2. Air breakthrough performance

Altering the traditional synthesis method [19] resulted in a Ag-ETS-10-HD adsorbent with a higher bulk density (compared to Ag-ETS-10-R) that was packed more efficiently in the column. Two comparative breakthrough experiments of air separation were performed using the same bed volume for Ag-ETS-10-R and Ag-ETS-10-HD adsorbents.

#### 3.2.1. O_2 production using a low density bed of Ag-ETS-10-R

Fig. 4a depicts the breakthrough concentration profiles for O_2, Ar and N_2 when air passed through the column packed with

Ag-ETS-10-R. During the experiment an argon-free oxygen product was detected on the 9th min (O_2 breakthrough). At the onset of argon breakthrough the bed was producing high purity oxygen for at least 2 min. Fig. 4b shows the outlet gas flow rate profile as a function of time. As the air was fed into the bed, the outlet flow decreased dramatically due to the adsorption step of N_2, Ar and O_2. The outlet flow remained at minimum value (~10 mL/min) during a period of 9 min as helium within the column was replaced by the air components. Pure oxygen started eluting immediately after. The N_2 breakthrough started at 13.5 min. The two step-changes in the outlet flow rate coincided with the breakthrough times of O_2 and N_2 (the two main constituents of air). Argon breakthrough was observed (as seen in Fig. 4a) between the breakthrough of O_2 and N_2. At 17 min, the concentration of N_2, O_2, and Ar in the outlet gas approached the feed gas composition, indicating that the Ag-ETS-10-R adsorbent has reached adsorption equilibrium with air.

The mean breakthrough times for O_2 and N_2 as described by Eq. (2) are represented by dashed lines in Fig. 4b. For Ar the breakthrough time was chosen at the data point where its concentration was less or equal to 2%.

3.2.2. Calculation of O_2 recovery

To calculate the amount of the recovered high purity oxygen, the outlet flow rate of the bed was integrated over the oxygen eluting time period (between the time of initial O_2 eluting and the time

(a)

(b)
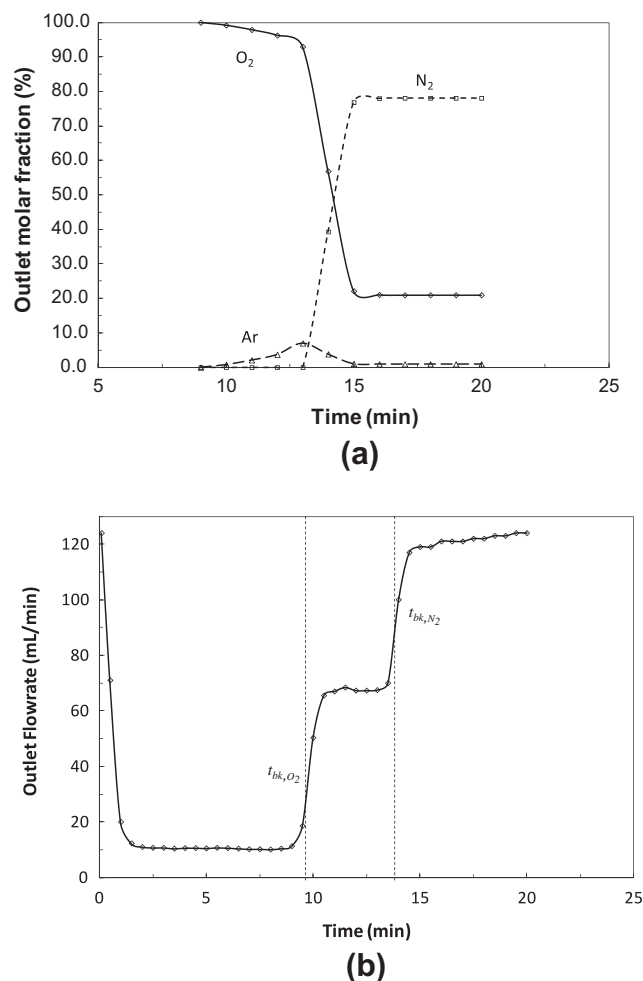
Fig. 4. Profiles of (a) breakthrough curves of air components and (b) gas flow rate in the outlet stream on Ag-ETS-10-R fixed-bed column (ρ_b = 1.12 g/cm^3). Air composition at feed is 78% N_2, 21% O_2 and 1% Ar. Flow rate is equal to 120 mL/min at 101.3 kPa and 25 °C (column conditions).

when argon concentration is not higher than 2%). In the case of Ag-ETS-10-R this interval was equal to 2 min.

During this 2 min time interval, a total of 87 mL of high purity O_2 (101.3 kPa and 25 °C) was recovered from the total gas fed into the column until the Ar breakthrough time. Thus, the pure oxygen (99+%) recovery was equal to 31.4%:

$$\% \text{ Recovery of pure } O_2 = \frac{\text{volume of produced pure } O_2}{\text{volume of } O_2 \text{ fed up to this step}} \times 100 \tag{9}$$

3.2.3. O_2 production using a Ag-ETS-10-HD bed

Fig. 5a shows the breakthrough concentration profiles for O_2, Ar and N_2 when air passed through the column filled with the high-density adsorbent Ag-ETS-10-HD. Breakthrough time values for air components were higher compared to the low density adsorbent. Breakthrough times increased as the bed density increased based on Eq. (2).

Argon-free oxygen product was detected at 15 min. The bed continued to produce high purity oxygen for a period of 3 min. During this 3 min interval, a total amount of 186 mL of high purity O_2 at 101.3 kPa and 25 °C was obtained. At 23 min, the nitrogen started eluting from the column. At 32 min, the molar fractions of N_2, O_2, and Ar in the outlet gas reflected the adsorption equilibrium of Ag-ETS-10-HD adsorbent with the feed gas.
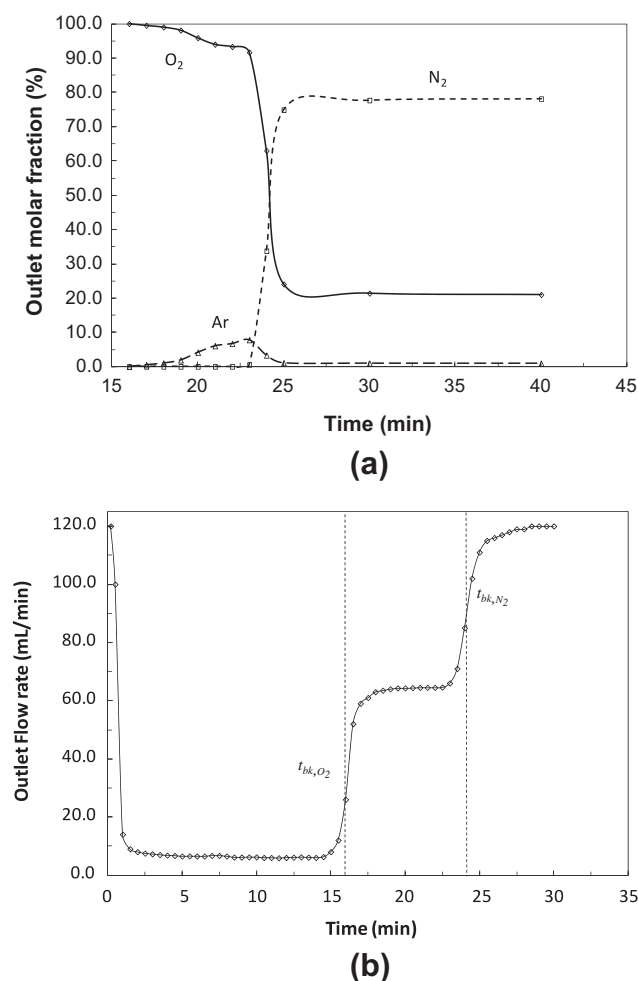
Table 2
Experimental breakthrough times and pure O_2 recoveries for air separation at 101.3 kPa and 25 °C using Ag-ETS-10-R and Ag-ETS-10-HD adsorbents.

Bed density (g/cm^3)	Experimental breakthrough times (min)			O_2 recovery (based on Eq. (6)) (%)	Experimental O_2 recovery (%)
	O_2	Ar	N_2		
1.12	9.6	11.0	14.0	33.1	31.4
1.45	16.0	19.0	24.0	39.3	38.9

Fig. 5b shows the profile of the outlet gas flow rate for the high density Ag-ETS-10-HD bed. High purity oxygen eluted after 15 min with a mean breakthrough time of 16 min. Nitrogen mean breakthrough time was at 24 min. During this experiment the amount of high purity O_2 was 186 mL at 101.3 kPa and 25 °C. Thus, the recovery rate of pure oxygen was equal to 38.9%. This is significantly higher compared to the low density Ag-ETS-10-R adsorbent recovery rate (Table 2). From the comparison of the breakthrough times values (Table 2), the calculated values for the coefficient $[(t_{bk,Ar} - t_{bk,O_2})/t_{bk,Ar}]$ (i.e., relative time lapse for pure O_2 production) in Eqs. (6) and (7) were equal to 0.16 and 0.11 for Ag-ETS-10-HD and Ag-ETS-10-R beds, respectively. This difference in values confirms the enhanced performance of the high density adsorbent bed and shows higher recovery for pure O_2 compared to the low density adsorbent.
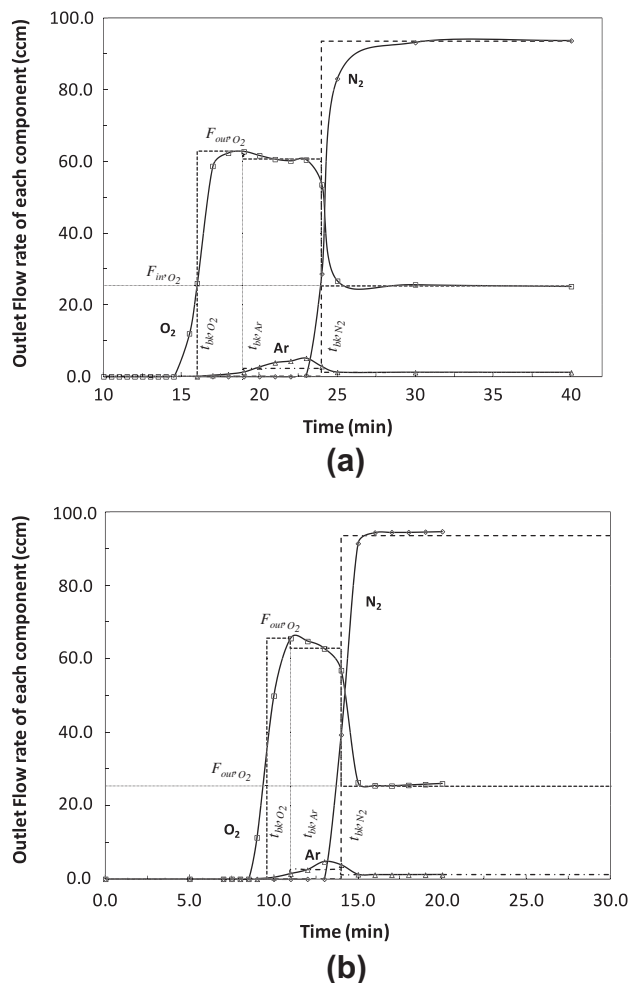

Fig. 5. Profiles of (a) breakthrough curves of air components and (b) gas flow rate in the outlet stream on Ag-ETS-10-HD fixed-bed column (ρ_b = 1.45 g/cm³). The air composition and flow rate are the same as in Fig. 4.

Fig. 6. Flow rates of O_2, Ar and N_2 in the outlet of a fixed-bed column packed with (a) Ag-ETS-10-HD and (b) Ag-ETS-10-R adsorbents. Dashed lines represent rectangular mass transfer zones (shock wave approximation). The air composition and flow rate are the same as in Fig. 4.

Table 3
Ternary adsorption capacities of N_2, O_2 and Ar predicted by ideal adsorption solution theory based on the Langmuir parameters[a] of single isotherms of Ag-ETS-10-R and Ag-ETS-10-HD at 25 °C. Adsorption affinities (q^*_{Ar}/C_{Ar} and $q^*_{O_2}/C_{O2}$) are calculated with air composition (78.0% N_2, 21.0% O_2, 1.0% Ar) at 25 °C and 100 kPa.

	$q^*_{N_2}$	$q^*_{O_2}$ $10^2 \times$ mmol/g	q^*_{Ar}	q^*_{Ar}/C_{Ar}	$q^*_{O_2}/C_{O2}$ cm^3/g	$1 - K^*_{O_2}/K^*_{Ar}$
Ag-ETS-10-R	47	3.6	0.20	4.9	4.3	0.12
Ag-ETS-10-HD	49	2.7	0.17	4.2	3.1	0.26

[a] $[q_{max,j} \text{ (mmol/g)} \; b_j \times 10^2 \text{ (kPa}^{-1})]_{Ads}$ with $j = N_2, O_2, Ar$: $\begin{bmatrix} 0.59 & 4.6 \\ 0.82 & 0.32 \\ 0.89 & 0.37 \end{bmatrix}_R$; $\begin{bmatrix} 0.65 & 4.5 \\ 1.02 & 0.27 \\ 1.00 & 0.38 \end{bmatrix}_{HD}$.

Fig. 6a shows the corresponding outlet flow rates of N_2, O_2 and Ar for the column filled with the high density adsorbent. The O_2 flow rate exceeded the corresponding value in the air feed (F_{in,O_2}). Once it reached its maximum value (F_{out,O_2}) the O_2 flow rate decreased slightly as Ar started eluting from the column. Finally, O_2 flow rate decreased abruptly during the breakthrough time of N_2 up until it reached the corresponding O_2 rate in the air feed.

The individual flow rate profiles of N_2, O_2 and Ar can be represented ideally by rectangular profiles (shock wave approximation). The O_2 recovery as described by the two terms in Eq. (6) corresponds to the rectangular areas that represent the produced O_2 ($F_{out,O_2} \times [t_{bk,Ar} - t_{bk,O_2}]$) and the O_2 fed into the bed ($F_{in,O_2} \times t_{bk,Ar}$). The O_2 recovery calculated based on Eq. (6) was 39.3%. This is an equivalent value of the experimental recovery obtained by the integration of the O_2 flow rate profile (Table 2).

Fig. 6b shows the outlet flow rates for N_2, O_2 and Ar for air separation through the low density Ag-ETS-10-R column. The relative time lapse for pure O_2 production [($t_{bk,Ar} - t_{bk,O_2})/t_{bk,Ar}$] was shorter compared to Ag-ETS-10-HD. Thus, the pure O_2 recovery obtained with the low density bed was lower than the recovery obtained with the high density material (Table 2).

Besides the effect of increased granule and bed bulk density, an additional contribution to a higher pure O_2 recovery can be associated with the larger adsorption capacity obtained for Ag-ETS-10-HD in comparison to Ag-ETS-10-R (Fig. 3). The increase of individual adsorption capacities, in particular the increase of N_2 capacity reduced the amount of O_2 remaining on the ternary equilibrium adsorption mixture. The prediction of the ternary equilibrium mixture using the Ideal Adsorbed Solution Theory (IAST) model showed that O_2 capacity decreased for the higher density material more than 25% (Table 3). The coefficient values ($1 - K^*_{O_2}/K^*_{Ar}$) calculated in Table 3 indicate different contributions of each adsorbent material to the relative time lapse for pure O_2 elution [($t_{bk,Ar} - t_{bk,O_2})/t_{bk,Ar}$]. The high density adsorbent (Ag-ETS-10-HD) has a relatively longer period of pure O_2 production than the regular material (Ag-ETS-10-R). The increase of the relative time lapse for pure O_2 [($t_{bk,Ar} - t_{bk,O_2})/t_{bk,Ar}$] in Ag-ETS-10-HD contributes to a higher O_2 recovery.

An estimation using Eq.8 suggests that the effect of increasing bulk density would be able to contribute between 7% and 25% to the total O_2 recovery increase. Thus, the effect of an increased adsorption capacity of Ag-ETS-10-HD contributed relatively more to the total increase of O_2 recovery than the gain in bulk density.

4. Conclusions

A higher capacity Ag-ETS-10 adsorbent formed into a bimodal distribution of higher density granules was found to improve the performance of air separation for the production of argon-free oxygen. The density of an adsorbent bed containing high density Ag-ETS-10 was enhanced by 35%. Pure oxygen recovery was improved by using this high-density bed versus the low-density material used previously. In a process demonstration, 187 mL of high purity (99+%) oxygen was obtained over a 150 mL bed of high density Ag-ETS-10 granules using air at 101.3 kPa and 25 °C. The O_2 recovery rate approached 40%; a 10% increase from the recovery rate when using a low-density bed. In conclusion, both the increase in bulk density and adsorption capacity contributed to a higher pure O_2 recovery. Further improvements in oxygen recovery rate should be still possible through continued densification of the adsorbent granules.

References

[1] H.J.M. Burggraaf, A.J. Bouwmeester, H.J.M. Buggraaf, L. Cot, Fundamentals of Inorganic Membrane Science and Technology, first ed., Elsevier, New York, 1996.
[2] J. Ermsley, Oxygen. Natures building blocks: an A–Z guide to the elements, Oxford University Press, Oxford, UK, 2001.
[3] A. Leo, S.M. Liu, J.C. Diniz da Costa, Development of mixed conducting membranes for clean coal energy delivery, Int. J. Greenhouse Gas Control 3 (2009) 357–367.
[4] R. Dubettier, A. Guillard, M. Cognard, J.-P. Tranier, N. Perrin, Air separation unit: flexibility and energy storage, in: 2nd Oxyfuel Combustion Conference, Queensland, Australia, 12–16 September 2011.
[5] C. Kunze, S. De, H. Spliethoff, A novel IGCC plant with membrane oxygen separation and carbon capture by carbon-calcinations loop, Int. J. Greenhouse Gas Control 5 (2011) 1176–1183.
[6] D.K. Aidun, S.A. Martin, Effect of sulfur and oxygen on weld penetration of high-purity austenitic stainless steels, JMEPEG 6 (1997) 496–502.
[7] H.Y. Dang, J. Wang, S.S. Fan, The synthesis of metal oxide nanowires by directly heating metal samples in appropriate oxygen atmospheres, Nanotechnol. 14 (7) (2003) 738–741.
[8] H. Lee, Y.-S. Kang, P.S. Lee, J.-Y. Lee, Hydrogen plasma treatment on catalytic layer and effect of oxygen additions on plasma enhanced chemical vapor deposition of carbon nanotube, J. Alloys Comp. 330–332 (2002) 569–573.
[9] N. Gascoin, P. Gillard, A. Mangeot, A. Navarro-Rodriguez, Literature survey for a first choice of a fuel–oxidiser couple for hybrid propulsion based on kinetic justifications, J. Anal. Appl. Pyrolysis 94 (2012) 1–9.
[10] C. Ma, N. Verma, Moisture drydown in ultra-high-purity oxygen systems, J. IEST 41 (1) (1998) 13–15.
[11] A.R. Smith, J. Klosek, A review of air separation technologies and their integration with energy conversion processes, Fuel Process. Technol. 70 (2001) 115–134.
[12] T. Tsuru, S.-T. Hwang, Production of high-purity oxygen by continuous membrane column combined with PSA oxygen generator, Ind. Eng. Chem. Res. 33 (1994) 311–316.
[13] X. Zhu, S. Sun, Y. Cong, W. Yang, Operation of perovskite membrane under vacuum and elevated pressures for high-purity oxygen production, J. Membr. Sci. 345 (2009) 47–52.
[14] S.S. Hashim, A.R. Mohamed, S. Bhatia, Oxygen separation from air using ceramic-based membrane technology for sustainable fuel production and power generation, Renew. Sustain. Energy Rev. 15 (2011) 1284–1293.
[15] S.M. Hashim, A.R. Mohamed, S. Bhatia, Current status of ceramic-based membranes for oxygen separation from air, Adv. Colloid Interface Sci. 160 (2010) 88–100.
[16] Y.A. Abdel-Jawad, W.S. Abdullah, Design of maximum density aggregate grading, Constr. Build. Mater. 16 (2002) 495–508.

[17] S. Yamada, J. Kanno, M. Miyauchi, Multi-sized sphere packing in containers: optimization formula for obtaining the highest density with two different sized spheres, IPSJ Online Trans. 4 (2011) 126–133.

[18] M.W. Anderson, O. Terasaki, T. Ohsuna, A. Philippou, S.P. MacKay, A. Ferreira, J. Rocha, S. Lidin, Structure of the microporous titanosilicate ETS-10, Nature 367 (1994) 347–351.

[19] S.M. Kuznicki, Large-Pored Crystalline Titanium Molecular Sieve Zeolites US Patent 5.011.591, 1991.

[20] Determination of Tap Density, <http://www.iso.org> (accessed 01.10.12).

[21] M. Shi, J. Kim, J.A. Sawada, J. Lam, S. Sarabadan, T.M. Kuznicki, S.M. Kuznicki, Production of argon free oxygen by adsorptive air separation on Ag-ETS-10, AIChE (2012). http://dx.doi.org/10.1002/aic.13879.

[22] A. Malek, S. Farooq, Effect of velocity variation on equilibrium calculations from multicomponent breakthrough experiments, Chem. Eng. Sci. 52 (1997) 443–447.

[23] G. Kluge, T. Franke, R. Schollner, G. Nagel, Estimation of component loadings in fixed-bed adsorption from breakthrough curves of binary gas mixtures in nontrace systems, Chem. Eng. Sci. 46 (1991) 368–371.

[24] Z.X. Ji, B. Yilmaz, J. Warzywoda, A. Sacco, Hydrothermal synthesis of titanosilicate ETS-10 using Ti(SO4)(2), Micropor. Mesopor. Mater. 81 (2005) 1–10.